

pubs.acs.org/Macromolecules Article

Foundation of Network Forensics

Andrey V. Dobrynin,* Michael Jacobs, and Yuan Tian



Cite This: Macromolecules 2023, 56, 9289-9296



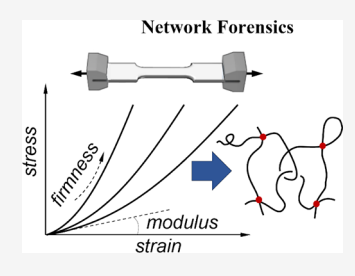
ACCESS I

Metrics & More

Article Recommendations

Supporting Information

ABSTRACT: We develop a forensic-like framework for network structural characterization based on an analysis of their nonlinear response to mechanical deformation. For model networks, this methodology provides information about the strand degree of polymerization between cross-links, the effective cross-link functionality, the contribution of loops and entanglements to network elasticity, as well as the fraction of stress-supporting strands. For networks with trapped entanglements, we identify a transition from cross-link-controlled to entanglement-controlled network elasticity with increasing degree of polymerization of network strands between cross-links and show how specific features of this transition are manifested in changes of entanglement and structural shear moduli characterizing different modes of network deformation. In particular, this



cross-link-to-entanglement transition results in saturation of the network shear modulus at small deformations and renormalization of the degree of polymerization of the effective network strands determining nonlinear elastic response in the strongly entangled networks. The developed approach enables the classification of networks according to their topology and effectiveness of stress distribution between network strands.

INTRODUCTION

The characterization of polymer networks remains a notorious challenge of polymer science. The main reason behind this is the random nature of polymerization reactions in which the outcome is difficult if not impossible to control, resulting in stochastic distribution of network structural elements (Figure 1) defining network mechanical properties. 1-5 The problem is further complicated by the lack of characterization techniques, which would allow one to dissect the network topology and establish specific contributions from structural elements. In the past, this was addressed by using the network modulus in the dry state to predict network swelling ability and, vice versa,

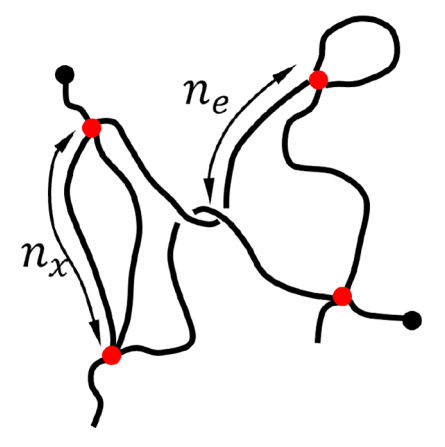


Figure 1. Schematic of a polymer network with cross-link functionality f = 4, degree of polymerization n_x between cross-links (red beads) and entanglements n_e containing various defects such as multiple strands, dangling loop and chain ends (black beads).

by using network swelling ratio as a measure of the cross-link density determining the shear modulus in the dry state. 1,2 Currently, the prediction of structure-property correlations is only possible for model networks with well-controlled structures of building blocks.^{7–9} This lack of progress fostered a trial-and-error approach in the design of elastomers and gels with specific applications in mind. Furthermore, advances in the synthesis of complex molecular architectures used as new building blocks in network design demand the development of a nondestructive flexible technique for the elucidation of structure–property correlations.^{3,12–14}

We address this problem by developing a forensic-like approach based on an analysis of the network mechanical response in the entire deformation range covering both linear and nonlinear regimes.³ In particular, we use a generalized form of the stress-deformation equation for uniaxially stretched networks which goes beyond the classical Mooney-Rivlin approach^{1,15,16} and allows extracting information about the degree of polymerization of network strands between crosslinks, network structural defects, and entanglements. The developed framework can be applied to any type of network and does not require assumptions about the types of structural defects^{5,9} by accounting their combined effect in the density of stress-supporting strands.

Received: April 4, 2023 Revised: October 20, 2023 Accepted: October 23, 2023 Published: November 15, 2023





The rest of the paper is organized as follows: we first illustrate the forensic approach on phantom networks of crosslinked linear precursor chains with different degrees of polymerization. This is accomplished by employing a nonlinear deformation to extract the degree of polymerization of network strands and quantify the contributions of effective cross-link functionality, loops, and dangling ends. After that, the developed framework is expanded to account for the contribution from trapped entanglements to the mechanical response of the network. This extension allows us to identify a transition to entanglement-controlled network elasticity and correlate this cross-link-to-entanglement transition with changes in the shear and entanglement modulus as the degree of polymerization of network strands between cross-links increases. The decoded structural information is then utilized to classify networks based on the network topology and effectiveness of stress distribution between network strands.

FORENSICS OF POLYMER NETWORKS

Phantom Networks. We begin the discussion of the forensic approach by analyzing the nonlinear deformation of phantom networks. The stress-deformation curves were obtained in molecular dynamics simulations of networks made by cross-linking noninteracting bead–spring precursor chains having degrees of polymerization N=401 and 1025 with density $\rho=0.85$ σ^{-3} of beads of diameter σ . The beads are connected by bonds with lengths of $l=0.965\sigma$. The chain bending constant is set to K=1.5 resulting in the Kuhn length $b_K=2.46\sigma$. A network was made by connecting every n_x -th bead, starting from the $(n_x/2)$ -th bead from a chain end to a similar neighboring bead on the other chain by a bond (Figure 2). The implemented cross-linking procedure produced

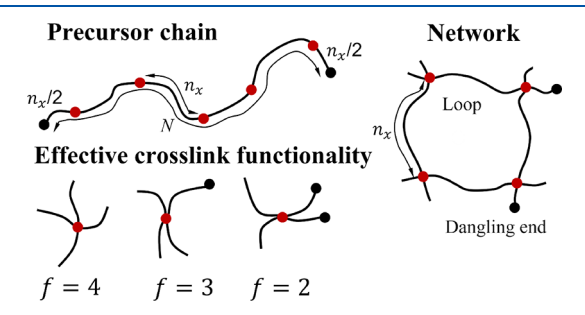


Figure 2. Phantom networks. Schematic representation of precursor chain, resultant network, and cross-links with varying effective functionality. Dangling ends and cross-linkable monomers are shown by black and red dots, respectively.

networks with tetrafunctional cross-links and a narrow distribution of the strand degree of polymerization (DP) having dispersity D < 1.02. We performed simulations of networks with the number of bonds between cross-links $n_x = 15-100$. The simulation details, specific forms of the bond and interaction potentials, cross-linking method, and network deformation protocol are described in the Supporting Information.

Figure 3 shows the dependence of the true stress, $\sigma_{\text{true}}(\lambda)$, on the deformation ratio λ for phantom networks undergoing uniaxial deformations at a constant volume. For all curves presented in this figure, the linear deformation regime is followed by a strong strain-stiffening. The expression for the stress-deformation curve, describing phantom networks made of strands with finite bending rigidity, is derived by considering

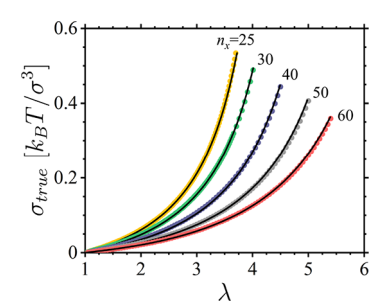


Figure 3. Dependence of the true stress $\sigma_{\rm true}$ on elongation ratio λ obtained in simulations of phantom networks made by cross-linking precursor chains with DP = 1025 in a melt state with monomer density $\rho = 0.85\sigma^{-3}$ at different values of n_x shown by filled circles of different colors: 25 (yellow), 30 (green), 40 (violet), 50 (gray), and 60 (pink). The lines are the best fits to eq 1 with G and G considered as fitting parameters (Table S1).

individual network strands as nonlinear springs, which results in the following expression for true stress^{3,17,18}

$$\sigma_{\text{true}}(\lambda) = (\lambda^2 - \lambda^{-1}) \frac{G}{3} \left[1 + 2 \left(1 - \frac{\beta(\lambda^2 + 2\lambda^{-1})}{3} \right)^{-2} \right]$$
(1)

The functional form of eq 1 is defined by the structural shear modulus, G, accounting for the elastic response of the stress-supporting strands and by the strain-stiffening (firmness) parameter, β . Parameter β describes the extensibility of the network strands

$$\beta \equiv \langle R_{\rm in}^2 \rangle / R_{\rm max}^2 = \alpha \left(1 - \frac{\alpha}{2} \left(1 - \exp\left(-\frac{2}{\alpha} \right) \right) \right) \tag{2}$$

with the number of n_x bonds between cross-links and the ratio of the initial mean-square end-to-end distance $\langle R_{\rm in}^2 \rangle$ to its fully extended state with $R_{\rm max} = n_x l$. The strain-stiffening parameter is determined by the number of Kuhn segments with length b_K per network strand, $\alpha^{-1} = R_{\rm max}/b_K$.

In phantom networks, the structural shear modulus includes contributions from stress-supporting strands between cross-links with average functionality $\langle f \rangle$, dangling ends, and loops ¹⁸:

$$G = \frac{G_m}{n_x} \frac{\langle R_{\rm in}^2 \rangle}{b_K R_{\rm max}} \left(1 - \frac{2}{\langle f \rangle} \right) C_{\rm loop} \left(1 - \frac{n_x}{N} \right)$$
(3)

where $G_m = \rho k_B T$ is the monomeric shear modulus defined by the monomer (bead) number density ρ and the thermal energy k_BT (k_B is the Boltzmann constant and T is the absolute temperature) and the coefficient C_{loop} accounts for loop contributions. The factor $1 - n_x/N$ describes the decrease in the density of the stress-supporting strands by two dangling ends per precursor chain $n_x/2$ beads each as illustrated in Figure 2. It is important to point out that the dangling ends not only change the density of the stress-supporting strands but also reduce the effective cross-link functionality when a cross-linkable monomer in the middle of the precursor chain is connected with an identical end monomer or when two crosslinkable end monomers form a bond (Figure 2). This effect is accounted for by using the average value of the cross-link functionality $\langle f \rangle$ which depends on the number of cross-links per chain $N_c = N/n_x$ and for tetrafunctional cross-links with f =4 is given by 18

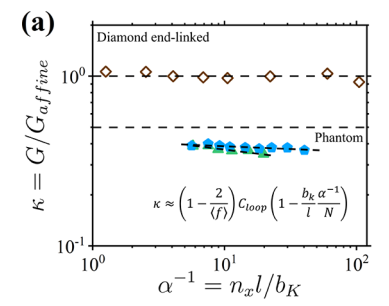
$$\langle f \rangle = 4 - \frac{2(N_c + 2)}{N_c^2 - 2N_c + 4}$$
 (4)

For long precursor chains, $N_c = N/n_x \gg 1$, the expression for $\langle f \rangle$ reduces to $\langle f \rangle \approx f$.

Analysis of eq 3 points out that we can introduce a quality factor, κ , that describes the network topology and the effectiveness of the network structure in redistributing stress. It is defined as the ratio of the network modulus G to the defect-free affine network model, G_{affine} , in which the stress is evenly divided between all network strands 1,19

$$\kappa = \frac{G}{G_{\text{affine}}} = \frac{Gb_K}{G_m l \beta} = \left(1 - \frac{2}{\langle f \rangle}\right) C_{\text{loop}} \left(1 - \frac{n_x}{N}\right)$$
 (5)

Thus, the parameter κ depends on the effective cross-link functionality, loop factor, and fraction of the monomers belonging to the stress-supporting strands which all together uniquely describe a network topology. Figure 4a shows the



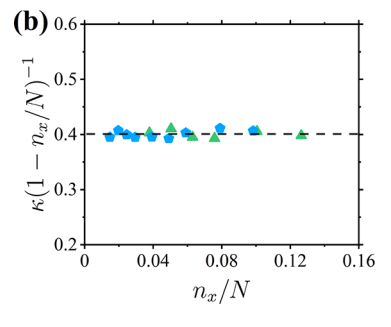


Figure 4. Self-similar networks. Dependence of quality factor $\kappa = G/G_{\rm affine}$ on the number of Kuhn segments per network strand, $\alpha^{-1} = n_x l/b_K$ for end-cross-linked diamond networks (open rhombs) and networks made by cross-linking precursor chains consisting of 401 (green triangles) and 1025 (blue pentagons) beads. (b) Reduced quality factor $\kappa (1-n_x/N)^{-1}$ as a function of n_x/N .

dependence of κ on the number of Kuhn segments per network strand for diamond networks ²⁰ and networks made by cross-linking linear chains with tetrafunctional cross-links. For diamond networks, $\kappa=1$ remains constant, independent of the number of Kuhn segments between cross-links. Thus, diamond networks can be regarded as the perfect network with maximum efficiency for stress distribution equivalent to that in the affine network model.

For networks of phantom linear chains, however, κ monotonically decreases with increasing the number of Kuhn segments between cross-links due to the increased fraction of monomers belonging to dangling ends. This decrease in κ can be eliminated by removing the contribution from dangling ends by multiplying κ by a factor of $(1 - n_x/N)^{-1}$ as confirmed in Figure 4b. Thus, for linear chain networks, the product of

the cross-link functionality coefficient and loop factor remains constant and equal to 0.40 ± 0.01 . This points out that these network elements support the stress with an efficiency of 40%. The constant value of the reduced quality factor, independent of the number of Kuhn segments per network strand, points out that the stress-supporting scaffold has a self-similar structure with a proportional distribution of beads between different network structural elements.

This self-similarity of the networks creates an opportunity to decode the network structural organization by analyzing their deformation curves. To proceed further, we can rewrite the expression for the network structural modulus as follows

$$G = G_m \frac{\beta}{\alpha} \left(1 - \frac{2}{\langle f \rangle} \right) C_{\text{loop}} \left(\frac{1}{b_K} \alpha - \frac{1}{N} \right)$$
(6)

In eq 6, α is used instead of the number of bonds n_x between cross-links since its actual value is a priori unknown, while α can be obtained by solving eq 2 for a known value of the firmness parameter β . Figure 5a shows the dependence of the

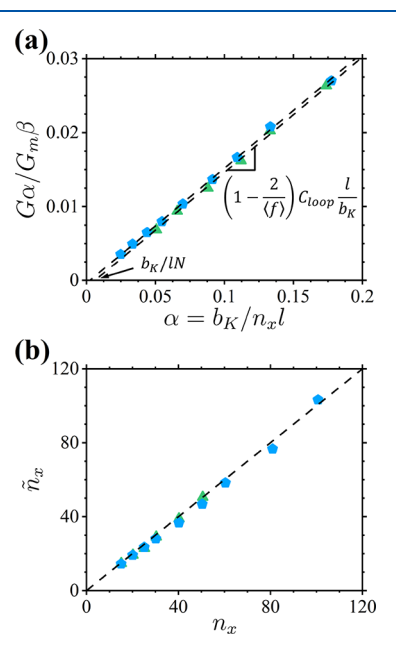


Figure 5. (a) Normalized structural modulus $G\alpha/G_m\beta$ as a function of parameter α for phantom networks made by cross-linking precursor chains consisting of 401 (green triangles) and 1025 (blue pentagons) beads and $G_m = 0.85k_BT/\sigma^3$. Dashed lines are the best linear fits given by y = 0.156x - 0.00098 (green triangles), y = 0.156x - 0.00040 (blue pentagons). (b) Dependence of the estimated number of bonds between cross-links \tilde{n}_x on the true value of n_x for phantom networks made by cross-linking precursor chains with N = 401 (triangles) and 1025 (pentagons). Dashed line corresponds to $\tilde{n}_x = n_x$.

normalized structural modulus $G\alpha/G_m\beta$ on parameter α for phantom networks with the degree of polymerization of the precursor chains equal to 401 and 1025. Both data sets follow straight lines with identical slopes and different values of the intercepts. From the intercept values, we estimate the degree of polymerization of the precursor chains to be 408 and 998. Finally, using the known ratio $b_K/l=2.56$ and the values for α determined by numerically solving eq 2, we obtain the number of bonds in the network strands between cross-links $\tilde{n}_x = b_K/l\alpha$. We introduce \tilde{n}_x to distinguish it from the actual number of bonds n_x fixed during the network cross-linking procedure. The

calculated values of \tilde{n}_x are within 8% of the actual n_x values (Figure 5b and Table S1).

We use the values of \tilde{n}_x and N to calculate $\langle \tilde{f} \rangle$ and compare it with $\langle f \rangle$ directly determined from analysis of the network structure (Figure 6a). These two values exhibit good

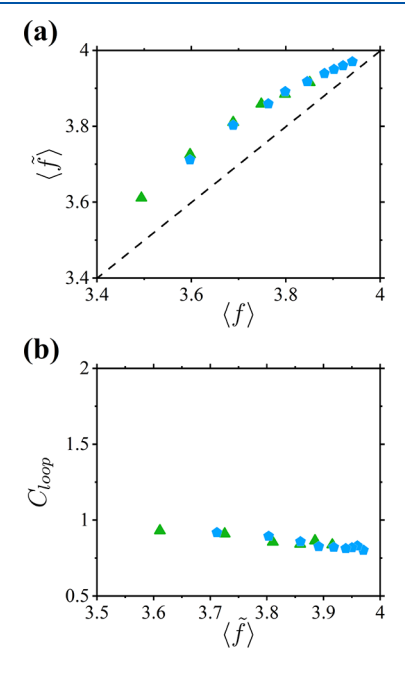


Figure 6. (a) Dependence of the estimated average value of cross-link functionality $\langle \tilde{f} \rangle$ calculated using eq 4 on the true value of $\langle f \rangle$ obtained from structural analysis of phantom networks made by cross-linking precursor chains with N=401 (triangles) and 1025 (pentagons). Dashed line corresponds to $\langle \tilde{f} \rangle = \langle f \rangle$. (b) Dependence of the loop coefficient C_{loop} on the average cross-link functionality $\langle \tilde{f} \rangle$ for linear chain networks. Symbol notations are the same as in panel (a).

agreement with a maximum difference of $\sim 3.5\%$. The obtained slopes in Figure 5a reproduce the value of the reduced κ parameter 0.40 \pm 0.01 for $b_K/l=2.56$. Taking this into account, we can estimate the loop coefficient and its dependence on the average cross-link functionality as follows

$$C_{\text{loop}} \approx 0.4 \frac{\langle f \rangle}{\langle f \rangle - 2}$$
 (7)

where the average cross-link functionality $\langle f \rangle$ is given by eq 4. The results of these calculations are summarized in Figure 6b. The loop coefficient $C_{\rm loop}$ decreases with increasing $\langle \tilde{f} \rangle$ in accordance with eq 7. Note that for the infinitely long precursor chains, the loop coefficient is equal to $C_{loop} \approx 0.80 \pm 0.02$. This estimate of the loop coefficient takes into account all types of loops rather than the particular types used in previous analytical calculations of the loop contributions. ^{9,21}

Entangled Networks. In real networks, excluded volume interactions between strands preclude their crossing, producing trapped entanglements. To highlight the differences between real and phantom networks and demonstrate the applicability of the forensic approach, we use molecular dynamics simulations to study the mechanical properties of coarsegrained networks made by cross-linking melts of entangled chains. The melts of precursor chains with DPs N=401 and 1025 equilibrated at bead density $\rho=0.85$ σ^{-3} and degree of polymerization between entanglements $n_e=27.5$ were cross-linked by a procedure similar to that used for cross-linking

phantom chains (Supporting Information). Simulations covered networks with $n_x = 15-150$. The excluded volume interactions between chains slightly increase the chain Kuhn length to $b_K = 2.82\sigma$ which corresponds to the effective bending constant K = 1.74 larger than the bare value K = 1.5. Therefore, to highlight differences in the mechanical properties of entangled and phantom networks, we performed simulations of phantom networks with identical cross-link topologies by turning off the nonbonded interactions and increasing the bending constant to K = 1.74 to maintain the strand statistics to be identical to that in networks of interacting chains.

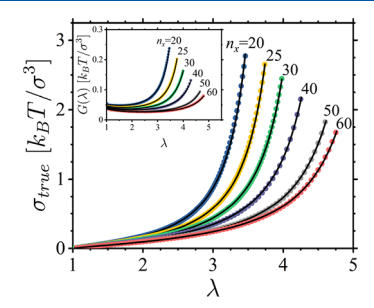


Figure 7. Dependence of the true stress $\sigma_{\rm true}$ on elongation ratio λ obtained in simulations of entangled networks made by cross-linking precursor chains with 1025 in a melt state with monomer density $\rho=0.85~\sigma^{-3}$ at different values of n_x shown by filled circles of different colors: 20 (blue), 25 (yellow), 30 (green), 40 (violet), 50 (gray), and 60 (pink). The lines are the best fits to eq 7 with G_e , G, and G0 considered as fitting parameters (Table S2). Inset shows the dependence of the deformation-dependent modulus (Mooney stress) $G(\lambda) = \sigma_{\rm true}(\lambda)/(\lambda^2 - \lambda^{-1})$.

Figure 7 shows stress—elongation curves of the uniaxially stretched entangled networks that are described by the following nonlinear equation of state^{3,17,18}

$$\sigma_{\text{true}}(\lambda) = (\lambda^2 - \lambda^{-1}) \left(\frac{G_{\epsilon}}{\lambda} + \frac{G}{3} \left[1 + 2 \left(1 - \frac{\beta(\lambda^2 + 2\lambda^{-1})}{3} \right)^{-2} \right] \right)$$
(8)

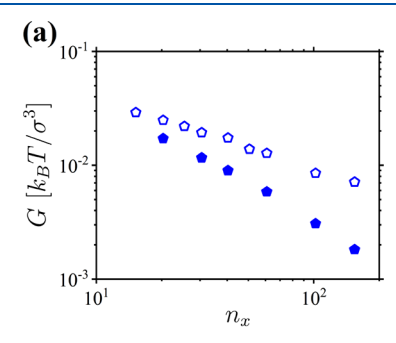
where the term with entanglement shear modulus, G_v accounts for contribution from the trapped entanglements. The complete set of fitting parameters G_v , G_v , and g_v for the stresselongation curves for the studied entangled and phantom networks presented in the Supporting Information is summarized in Table S2.

The structural shear modulus for entangled networks is represented as

$$G = \frac{G_m}{n_x} \frac{\langle R_{\rm in}^2 \rangle}{b_K R_{\rm max}} \left(1 - \frac{2}{f} \right) \left(1 \pm \frac{n_x}{N_{\rm eff}} \right)$$
(9)

where we included $C_{\rm loop}$ and the renormalization of the cross-link functionality into the definition of the factor $(1 \pm n_x/N_{\rm eff})$. Due to the complex topological structure of entangled networks, it is impossible to separate the contributions of loops and the renormalization of cross-link functionality from the correction factor associated with the fraction of beads (monomers) in the stress-supporting strands controlled by an effective density of defects $1/N_{\rm eff}$. Note that depending on the relative concentrations of different structural elements, their net effect on the network elasticity could be positive or

negative, as reflected by the \pm sign in eq 9. Entanglements enhance network mechanical strength, resulting in a positive reinforcement of structural modulus, while dangling ends and loops provide a negative effect on reducing network modulus. This is illustrated in Figure 8a comparing structural shear



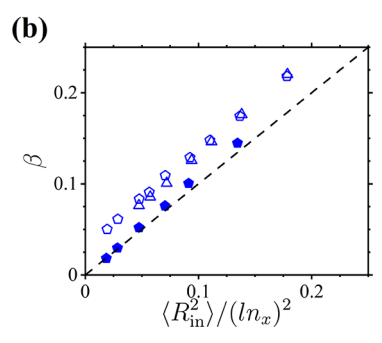


Figure 8. (a) Dependence of the structural shear modulus G on the number of bonds between cross-links n_x for entangled (open pentagons) and phantom (filled pentagons) networks with N=1025. (b) Dependence of the firmness parameter β on the value of the parameter $\langle R_{\rm in}^2 \rangle / (\ln_x)^2$ calculated by using simulation data for network strands in the undeformed state for entangled networks with N=1025 (open pentagons) and 401 (open triangles). Filled symbols represent corresponding phantom networks with N=1025.

moduli of the entangled and phantom networks with the identical topology of the cross-linked chains. The difference between phantom and entangled network modulus quantifies the silent effect of trapped entanglements in renormalizing the structural modulus of entangled networks.

Another feature separating entangled and phantom networks is the renormalization of the number of bonds of the network strands between cross-links, which defines the crossover to the nonlinear network deformation regime, such that the network strain-stiffening (firmness) parameter β obtained from the fitting of the stress—elongation curves (Figure 7) is different from the value estimated by using $\langle R_{\rm in}^2 \rangle$ calculated for the undeformed network strands (Figure 8b). Thus, our method for determining the network structural parameters should be modified to account for this renormalization. This is done by rewriting eq 9 for the structural modulus as follows

$$\frac{G\alpha}{G_{m}\beta} = \frac{\langle R_{\rm in}^{2} \rangle}{\langle R_{\rm in}^{2}(\beta) \rangle} \frac{n_{x}(\beta)}{n_{x}} \left(1 - \frac{2}{f}\right) \left(\frac{l}{b_{K}} \frac{n_{x}(\beta)}{n_{x}} \alpha \pm \frac{1}{N_{\rm eff}}\right)$$
(10)

where $\langle R_{\rm in}^2(\beta) \rangle$ is the mean square end-to-end distance of an undeformed chain section with the number of bonds $n_x(\beta)$ calculated from eq 2 using the fitting value of the firmness parameter β . Taking into account this transformation, the slope

$$a = \left(1 - \frac{2}{f}\right) \frac{1}{b_K} \frac{\beta(n_x)}{\beta} \tag{11}$$

in the plot of the l.h.s of the eq 10 as a function of the parameter α includes information about the number of bonds between cross-links n_x through parameter $\beta(n_x) = \langle R_{\rm in}^2 \rangle / l^2 n_x^2$ —the strain-stiffening parameter corresponding to the strands with n_x bonds between cross-links. Solving eq 11 for $\beta(n_x)$, we have

$$\beta(n_x) = \left(1 - \frac{2}{f}\right)^{-1} \frac{b_K}{l} a\beta \tag{12}$$

This value of $\beta(n_x)$ is used to obtain n_x by numerically solving eq 2 for $\alpha(n_x)$ and substituting it into the expression $n_x = b_K / l\alpha(n_x)$. The intercept value

$$c = \frac{\langle R_{\rm in}^2 \rangle}{\langle R_{\rm in}^2(\beta) \rangle} \frac{n_x(\beta)}{n_x} \left(1 - \frac{2}{f} \right) \frac{1}{N_{\rm eff}} = a\alpha \frac{n_x}{N_{\rm eff}}$$
(13)

provides information about the fraction of beads belonging to the different types of structural defects.

Figure 9a shows the normalized structural modulus, $G\alpha/G_m\beta$, as a function of parameter α . There are two clearly identifiable regimes that indicate a transition from cross-link-to entanglement-controlled network elasticity—cross-link-to-entanglement transition. In particular, the data for entangled networks with different degrees of polymerization of the precursor chains collapse for $\alpha < 0.11$, corresponding to the interval $n_x > n_e$. In this entanglement-dominated regime, the structural shear modulus is given by

$$G \approx 0.17 G_{\text{m}} \beta = (1 - 2f^{-1}) G_{\text{m}} \beta l / b_{\text{k}}$$
 (14)

In writing eq 14, we take into account that the numerical coefficient for the best fit is close to the value obtained by using the values of Kuhn length $b_K = 2.82\sigma$, bond length $l = 0.965\sigma$, and f = 4. Thus, in this regime, it appears that the structural shear modulus could be described in the framework of a defect-free phantom network model¹⁹ of the effective strands with the number of bonds between the entangled strands n_e and cross-linked strands n_x , as will be illustrated below.

For the interval $\alpha > 0.11$, the data sets split into two lines with two different positive intercept values (c-values) but identical values of the slope. The larger intercept value corresponds to the entangled network with the longer precursor chains, N=1025, in which the contribution of the dangling ends is smaller and the same density of entanglements leads to a stronger net effect on the network structural modulus. In this interval of parameters, the structural shear modulus is described in eq 10.

A monotonic increase of the normalized structural modulus, $G\alpha/G_m\beta$, with parameter α is observed for phantom networks with the identical topology of cross-links (Figure 9a). For such networks, the intercept with the α -axis occurs in the positive α range (negative c-value), pointing out the dominant role of the dangling ends. It is also worth pointing out that for phantom networks, the structural modulus, strain-stiffening parameter, and shear modulus at small deformations are smaller than the corresponding values for entangled networks with identical n_x (Table S2, Supporting Information). This highlights the enhancement of the network mechanical properties by

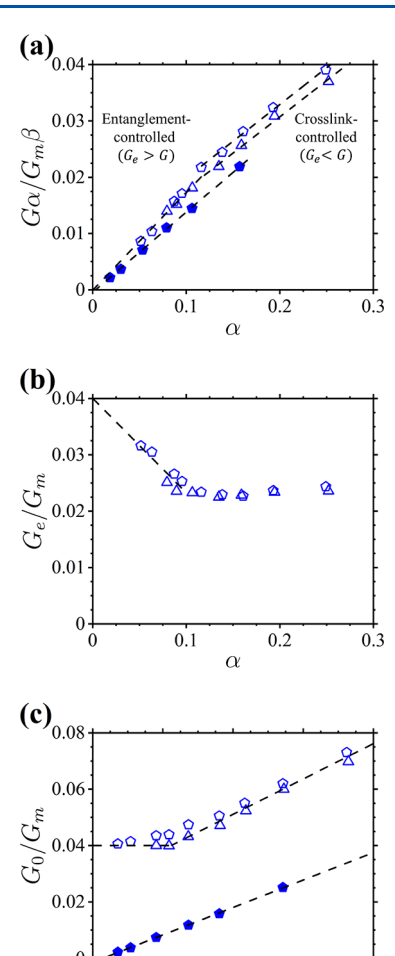


Figure 9. (a) Normalized structural modulus $G\alpha/G_m\beta$ as a function of parameter α for entangled networks made by cross-linking precursor chains with N=401 (open triangles) and 1025 (open pentagons) and $G_m=0.85k_BT/\sigma^3$, and for phantom networks (filled pentagons) obtained from entangled networks. Dashed lines are the best linear fits given by y=0.17x (open symbols) for $\alpha<0.11$, y=0.15x-0.0004 (filled symbols), y=0.13x+0.005 (open triangles), and y=0.13x+0.007 (open pentagons) for $\alpha>0.11$. (b) Dependence of the normalized entanglement modulus G_c/G_m on parameter α for entangled networks shown in panel a. (c) Normalized shear modulus at small deformations G_0/G_m ($G_0 \equiv G_c + G(1+2(1-\beta)^{-2})/3$) as a function of the ratio n_c/n_x . Dashed lines show general trends.

1.5

entanglements. This observation is in agreement with experimental studies of strongly entangled gels.²³

The entanglement shear modulus (Figure 9b) increases with decreasing value of the parameter α for the interval α < 0.11. Considering that the shear modulus at small deformations saturates (see Figure 9c) and is equal to the sum of the structural and entanglement moduli, $G_0 \approx G_e + G$, for $\beta \ll 1$, we can write down the following expression for the entanglement modulus

$$G_e \approx G_{av} - (1 - 2/f)G_m \beta l/b_K \tag{15}$$

where $G_{av} \approx 0.034 k_B T/\sigma^3$ is the plateau value of the shear modulus at small deformations in the saturation regime (Figure 9c). Note that the value of G_{av} is close to $G_m/n_e \approx 0.031 k_B T/\sigma^3$. The entanglement shear modulus has a weak minimum for $\alpha > 0.11$, where cross-links define network elasticity.

This finding calls into question the commonly held belief of continuous scaling of the network modulus, $G_0 \approx n_e^{-1} + n_x^{-1}$, a conviction that permeates the modern network literature ^{7,24} and textbooks. ^{19,25} In particular, our data show that the entanglement contributions (before and after cross-link-toentanglement transition) are qualitatively different (Figure 9). In the densely cross-linked networks with $n_x < n_e$, the increase of G and weak increase of G_e (Figure 9a,b) moduli with increasing cross-linking density is due to a decrease of entanglements in dangling ends combined with an enhancement of constraints imposed by cross-links on entanglement fluctuations. In the weakly cross-linked networks with $n_x > n_e$, these constraints are relaxed, and fluctuations of entanglements are like those in a melt of precursor chains. As the ratio n_e/n_x decreases, the entanglement modulus G_e monotonically increases toward the melt plateau value (Figure 9b), while the structural modulus decreases toward zero (Figure 9a). Note that the observed trend in dependence of the shear modulus at small deformations, G_0 , across entanglement-tocross-link transition (Figure 9c) is consistent with the experimental data for end-cross-linked PDMS networks⁸ replotted in Figure S3 (Supporting Information). Detailed comparison of the simulation and experimental data for G_0 , G_e G, and β in the networks undergoing cross-link-to-entanglement transition is discussed elsewhere.

We can use the data shown in Figure 9a to evaluate the number of bonds between cross-links, \tilde{n}_x , from the nonlinear network deformation. Note that here, as in the case of phantom networks, we use \tilde{n}_x to distinguish it from the n_x value expected from the cross-linking procedure. The results of these calculations are summarized in Figure 10. Above the transition,

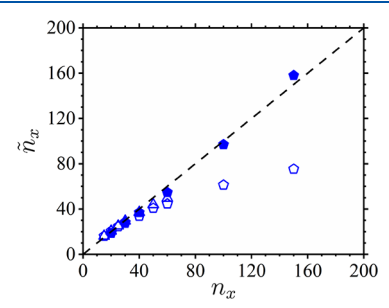


Figure 10. Dependence of the estimated number of bonds between cross-links \tilde{n}_x on the true value of n_x for entangled (open symbols) and phantom (filled symbols) networks made by cross-linking precursor chains with N=401 (triangles) and 1025 (pentagons). Dashed line corresponds to $\tilde{n}_x=n_x$.

 $\alpha > 0.11$, we use eqs 11 and 12 to calculate $\beta(\tilde{n}_x)$, the corresponding $\alpha(\tilde{n}_x)$ from eq 2, and the number of bonds $\tilde{n}_x = b_K/l\alpha(\tilde{n}_x)$. Below the transition in strongly entangled networks, $\alpha < 0.11$, the number of bonds \tilde{n}_x is calculated directly from α corresponding to the firmness parameter β . For networks with cross-link-controlled elasticity, $n_e > n_x$, $\tilde{n}_x \approx n_x$ as illustrated in Figure 10 and Table S2. The calculated values of the number of bonds, \tilde{n}_x deviate from the true values, n_x for strongly entangled strands, $n_e < n_x$ pointing out that for such long strands between cross-links, entanglements screen the true n_x value (Table S2). This indicates that for networks with entanglement-controlled elasticity, a proper analysis would require establishing the general relationship between the true number of bonds (or degree of polymerization) between cross-links and the value extracted from the firmness parameter. As a

starting point, we can use a plot shown in Figure 10 to elucidate such a relationship. The phantom networks again show a good agreement between \tilde{n}_x and n_x in the entire interval of studied n_x values as expected.

Figure 11 combines data for the quality factor, κ , quantifying the network topology for entangled, phantom, and diamond²⁰

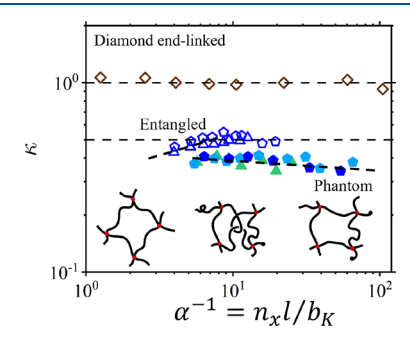


Figure 11. Mapping polymer networks with different topologies in terms of quality factor κ and number of Kuhn segments per network strand, α^{-1} . The analyzed networks include: end-cross-linked diamond networks (open rhombs), phantom networks (filled symbols), and entangled networks (open symbols). Insets illustrate the network mesh structure.

networks with different numbers of the Kuhn segments per network strand, α^{-1} . Diamond networks have the quality factor $\kappa = 1$ independent of the number of Kuhn segments per network strand, pointing out the absence of dangling ends and equal partitioning of the applied stress between all network strands. For phantom networks, the κ -parameter monotonically decreases with an increasing number of Kuhn segments per network strand, highlighting that dangling ends soften the network in comparison with an ideal phantom network with the quality factor $\kappa = 0.5$ for cross-link functionality f = 4. However, for entangled networks, κ first increases with α^{-1} and then passes through a weak maximum, reflecting a dependence of the structural shear modulus on the number of Kuhn segments per network strand. The increase in the parameter κ is associated with the strengthening of the network by entanglements (see eq 9), while appearance of a maximum corresponds to a transition from cross-link-controlled to entanglement-controlled network elasticity with structural modulus given by eq 14.

CONCLUSIONS

We develop a forensic framework for the analysis of the network structure from the nonlinear mechanical response, which can be applied to both simulation and experimental data. The approach includes three main steps: (i) fit the nonlinear deformation curve by eq 8 to obtain structural modulus, entanglement modulus and strain-stiffening (firmness) parameter β ; (ii) solve eq 2 for the number of Kuhn segments per network strand; (iii) represent the data in the form of eqs 6 or 8 to obtain parameters describing network structural organization. By following these steps, we show how to determine the number of bonds or degree of polymerization of network strands between cross-links (Figures 5b and 10), the fraction of monomers belonging to stress-supporting strands, and the location of the transition between cross-link and entanglement-controlled network elasticity (cross-link-toentanglement transition) (Figure 9).

In the entanglement-controlled regime, we demonstrate that the degree of polymerization of the effective strands, which defines the network strain-stiffening response, has a degree of polymerization between those of entangled strands and strands between cross-links (Figure 10). Thus, entanglements renormalize the mechanical properties of network strands. These results challenge the current understanding of entanglements in polymer networks 19,22,26–31 and require further investigation.

For phantom networks, we use the forensic approach to obtain $C_{\rm loop}\approx 0.80\pm 0.02$ for infinitely long chains. Additionally, we investigated the effect of the dangling ends on the effective cross-link functionality and loop coefficient (Figure 6), which would be difficult to estimate by other means.

We believe that the simplicity of our forensic approach will make it a valuable tool for analyzing the experimental data for series of networks with linear and brush-like strands^{3,6,12} as illustrated in ref 18.

ASSOCIATED CONTENT

s Supporting Information

The Supporting Information is available free of charge at https://pubs.acs.org/doi/10.1021/acs.macromol.3c00612.

Computer simulation details and data analysis (PDF)

AUTHOR INFORMATION

Corresponding Author

Andrey V. Dobrynin — Department of Chemistry, University of North Carolina at Chapel Hill, Chapel Hill, North Carolina 27599, United States; orcid.org/0000-0002-6484-7409; Email: avd@email.unc.edu

Authors

Michael Jacobs — Center for Nanophase Materials Sciences, Oak Ridge National Laboratory, Oak Ridge, Tennessee 37830, United States; orcid.org/0000-0002-7255-3451 Yuan Tian — Department of Chemistry, University of North Carolina at Chapel Hill, Chapel Hill, North Carolina 27599, United States; orcid.org/0000-0002-7277-1408

Complete contact information is available at: https://pubs.acs.org/10.1021/acs.macromol.3c00612

Notes

The authors declare no competing financial interest.

ACKNOWLEDGMENTS

This work was supported by the National Science Foundation under the grant DMR 2049518.

REFERENCES

- (1) Treloar, L. R. G. The Physics of Rubber Elasticity. Clarendon Press: Oxford, 1975 DOI: 10.1063/1.3060678.
- (2) Flory, P. J. Principles of Polymer Chemistry. Cornell University Press: Ithaca, NY, 1971.
- (3) Sheiko, S. S.; Dobrynin, A. V. Architectural code for rubber elasticity: From supersoft to superfirm materials. *Macromolecules* **2019**, *52*, 7531–7546.
- (4) McKenna, G. B. Soft matter: rubber and networks. Rep. Prog. Phys. 2018, 81, No. 066602.
- (5) Flory, P. J. Network topology and the theory of rubber elasticity. *Br. Polym. J.* **1985**, *17*, 96–102.

- (6) Danielsen, S. P. O.; Beech, H. K.; Wang, S.; El-Zaatari, B. M.; Wang, X.; Sapir, L.; Ouchi, T.; Wang, Z.; Johnson, P. N.; Hu, Y.; Lundberg, D. J.; Stoychev, G.; Craig, S. L.; Johnson, J. A.; Kalow, J. A.; Olsen, B. D.; Rubinstein, M. Molecular characterization of polymer networks. *Chem. Rev.* **2021**, *121*, 5042–5092.
- (7) Dossin, L. M.; Graessley, W. W. Rubber elasticity and well-characterized polybutadiene networks. *Macromolecules* **1979**, 12, 123–130.
- (8) Patel, S. K.; Malone, S.; Cohen, C.; Gillmor, J. R.; Colby, R. H. Elastic-modulus and equilibrium swelling of poly(dimethylsiloxane) networks. *Macromolecules* **1992**, *25*, 5241–5251.
- (9) Zhong, M.; Wang, R.; Kawamoto, K.; Olsen, B. D.; Johnson, J. A. Quantifying the impact of molecular defects on polymer network elasticity. *Science* **2016**, 353, 1264–1268.
- (10) Zhang, Y. S.; Khademhosseini, A. Advances in engineering hydrogels. *Science* **2017**, *356*, No. eaaf3627.
- (11) Peppas, N. A.; Hilt, J. Z.; Khademhosseini, A.; Langer, R. Hydrogels in biology and medicine: from molecular principles to bionanotechnology. *Adv. Mater.* **2006**, *18*, 1345–1360.
- (12) Vatankhah-Varnosfaderani, M.; Daniel, W. F. M.; Everhart, M. H.; Pandya, A. A.; Liang, H. Y.; Matyjaszewski, K.; Dobrynin, A. V.; Sheiko, S. S. Mimicking biological stress-strain behaviour with synthetic elastomers. *Nature* **2017**, *549*, 497–501.
- (13) Vatankhah-Varnosfaderani, M.; Keith, A. N.; Cong, Y. D.; Liang, H. Y.; Rosenthal, M.; Sztucki, M.; Clair, C.; Magonov, S.; Ivanov, D. A.; Dobrynin, A. V.; Sheiko, S. S. Chameleon-like elastomers with molecularly encoded strain-adaptive stiffening and coloration. *Science* **2018**, *359*, 1509–1513.
- (14) Sheiko, S. S.; Everhart, M. H.; Dobrynin, A. V.; Vatankhah-Varnosfaderani, M. Encoding tissue mechanics in silicone. *Sci. Rob.* **2018**, *3*, No. eaat7175.
- (15) Mooney, M. A theory of large elastic deformation. J. Appl. Phys. 1940, 11, 582.
- (16) Rivlin, R. S. Large elastic deformations of isotropic materials. I. Fundamental concepts. *Philos. Trans. R. Soc. A* **1948**, 240, 459–490.
- (17) Dobrynin, A. V.; Carrillo, J.-M. Y. Universality in nonlinear elasticity of biological and polymeric networks and gels. *Macromolecules* **2011**, *44*, 140–146.
- (18) Dobrynin, A. V.; Tian, Y.; Jacobs, M.; Nikitina, E. A.; Ivanov, D. A.; Maw, M.; Vashahi, F.; Sheiko, S. S. Forensics of Polymer Networks. *Nat. Mater.* **2023**, *22*, 1394–1400.
- (19) Rubinstein, M.; Colby, R. H. *Polymer Physics*. Oxford University Press: New York, NY, 2003.
- (20) Carrillo, J.-M. Y.; MacKintosh, F. C.; Dobrynin, A. V. Nonlinear elasticity: from single chain to networks and gels. *Macromolecules* **2013**, *46*, 3679–3692.
- (21) Panyukov, S. Loops in polymer networks. *Macromolecules* **2019**, 52, 4145–4153.
- (22) Edwards, S. F.; Vilgis, T. A. The tube model theory of rubber elasticity. *Rep. Prog. Phys.* **1988**, *51*, 243–297.
- (23) Kim, J.; Zhang, G.; Shi, M.; Suo, Z. Fracture, fatigue, and friction of polymers in which entanglements greatly outnumber cross-links. *Science* **2021**, *374*, 212–216.
- (24) Duering, E. R.; Kremer, K.; Grest, G. S. Structure and relaxation of end-linked polymer networks. *J. Chem. Phys.* **1994**, *101*, 8169–8192.
- (25) Graessley, W. W. Polymeric Liquids & Networks: Structure and Properties. Garland Science: New York, 2004 DOI: 10.4324/9780203506127.
- (26) Higgs, P. G.; Gaylord, R. J. Slip-links, hoops and tubes: tests of entanglement models of rubber elasticity. *Polymer* **1990**, *31*, 70–74.
- (27) Kaliske, M.; Heinrich, G. An extended tube model for rubber elasticity: Statistical-mechanical theory and finite element implementation. *Rubber Chem. Technol.* **1999**, *72*, 602–632.
- (28) Rubinstein, M.; Panyukov, S. Elasticity of polymer networks. *Macromolecules* **2002**, *35*, 6670–6686.
- (29) Rubinstein, M.; Panyukov, S. Nonaffine deformation and elasticity of polymer networks. *Macromolecules* **1997**, *30*, 8036–8044.

- (30) Mergell, B.; Everaers, R. Tube models for rubber-elastic systems. *Macromolecules* **2001**, *34*, 5675–5686.
- (31) Davidson, J. D.; Goulbourne, N. A nonaffine network model for elastomers undergoing finite deformations. *J. Mech. Phys. Solids* **2013**, 61, 1784–1797.